26th ABCM International Congress of Mechanical Engineering
November 22-26, 2021. Florianópolis, SC, Brazil

COB-2021-0900
COMPARISON OF FRICTION PROPERTIES OF MATERIALS WITH DIFFERENT HARDNESS FOR CABLE RIDING ROBOTS' WHEELS

Marina Baldissera de Souza
Gustavo Queiroz Fernandes
Rodrigo de Souza Vieira
Lauro Cesar Nicolazzi
Universidade Federal de Santa Catarina, Departamento de Engenharia Mecânica, Centro Tecnológico, Campus Universitário - Trindade, CEP: 88.040-900, Florianópolis/SC - Brasil
marina.bs@posgrad.ufsc.br - gustavo.fernandes@posgrad.ufsc.br - rodrigo.vieira@ufsc.br - lauro.nicolazzi@ufsc.br

Roberto Kinceler
Alessandro Pedro Dadam
Celesc Distribuição S.A., Florianópolis/SC - Brasil
rkinceler@celesc.com.br - alessandropd@celesc.com.br

Abstract. *Robots for inspecting overhead power lines are designed to automate the inspection process, aiming to reduce the inspection time and enhance reliability. Most of the inspection robots travel along the power line conductors through wheels made of insulating materials. Besides protecting the robot's systems and components from an electric discharge, the wheel material must assure that the robot is able to accelerate, ride a slope and brake without overloading the traction motor. One way to check if the wheel material meets these requirements is measuring the friction coefficient between the surface of the wheel and the surface of a wire cable conductor. In this paper, two wheel's replicas of distinct material are field tested to establish the static friction coefficient and the rolling resistance coefficient between their surface and a real standard conductor cable. The wheel's materials are ABS plastic and Polyurethane of 50 Shore A hardness. The coefficients are measured by placing a wheel's replica on an aluminum conductor connecting two poles with different heights. One end of a rope parallel to the conductor is tied to the replica and the other end is attached to a recipient. The recipient mass is slowly augmented until the static equilibrium is broken. The coefficients are estimated from the recipient weight that broke the equilibrium. The static friction and rolling resistance coefficients define the maximum inclination that the robot can stay parked, the motor torque and the power dissipated during robot ride. These parameters are quantifiable and enable an objective comparison of the two materials. This way, the most adequate material to manufacture the robot wheels can be selected, presenting a compromise between consumption and riding capability.*

Keywords: *Friction on wire cable, field robotics, riding capability, power line inspection*

1. INTRODUCTION

An extent part of the medium-voltage energy supply grid in Brazil is covered by overhead power distribution lines (Prates *et al.*, 2019). The failure of energy utility companies in providing proper preventive and corrective maintenance on those extent grids may lead to inefficiency on energy distribution and, sometimes, to complete blackouts. The energy provision interruption represents both financial and life risks, once industries, hospitals, schools, and other systems are dependent on energy to work (Jenssen *et al.*, 2018). In addition, most of the Brazilian energy providers currently perform only visual inspections of distribution lines with walking patrol professionals. The human visual analysis can also be a source of uncertainty in the process, as it is susceptible to misinterpretation and wrong problem diagnosis (Prates *et al.*, 2019).

At first thought, drones could be a great solution for faster and more reliable inspections as they could cover large areas within minutes and take images of distribution line elements from a closer perspective. However, drones and other unmanned aerial vehicles (UAV's) have yet to surpass a series of challenges before being a feasible option (Shakhatreh *et al.*, 2019). UAV's usually have limited flying times between battery charges. Moreover, most of the distribution lines are located in urban areas and there may exist local regulations that limit the application of drones on those regions, such as maximum payload, minimum distance from buildings and people and requirement for trained and licensed professionals in order to operate them.

As a solution, energy companies have attempted to automate the inspection of overhead power lines through the development of inspection robots. Proof of those efforts are the number of works available in the literature regarding the development of inspection robots within the last ten years (Zhang *et al.*, 2020), (Wang *et al.*, 2019), (Gulzar *et al.*, 2018), (Mirallès *et al.*, 2018), (Chang *et al.*, 2017), (Qing *et al.*, 2016), (Mostashfi *et al.*, 2014), (Boje, 2014). Most of these works deal with the design of robotic systems that are in direct contact to the distribution line, with wheels riding over the aluminium conductors.

When designing robotic systems that move along cables, an important design requirement is the friction coefficient between robot wheel and wire. As described in the designs of the cable-crawler robot developed by Bühringer *et al.* (2010) and the Expliner robot (Debenest *et al.*, 2008), the first prototypes in both cases had slippage problem because a minimum friction coefficient was not met. In both cases, modifications on the material used for manufacturing the wheels had to be implemented, leading to rework and additional costs. The impact of friction on the performance of cable climbing robots is also superficially discussed for the design of SkySweeper (Morozovsky and Bewley, 2013) or the simulations carried out by Yifeng *et al.* (2011) to analyse how the driving wheel is related to robot's climbing capabilities. In any of those works, however, the authors also do not delve deeper into the numerical specification of the friction coefficient or how it could be estimated. In other works, such as the ones developed by Goncalves and Carvalho (2015), Yang *et al.* (2012), Li *et al.* (2009), Pouliot and Montambault (2008) and Nayyerloo *et al.* (2007), the friction forces are not even discussed.

Being able to numerically estimate the friction coefficients allows designers not only to guarantee there will not occur slippage during operation. It also allows engineers to calculate the required motor's torque and power more precisely and assertively, besides enabling a more robust control system. Moreover, with the development of manufacturing techniques and new materials, many design options may be considered during the conceptual design phases. Therefore, engineers must not only be able to quantitatively estimate the friction coefficients but also to have criteria that allow the selection of the most adequate solution among the available material options.

Considering the lack of studies on assessing numerically the friction forces between wires and cable climbing robot wheels and on selecting wheels material, the main objective of this paper is to propose some parameters to compare two different wheel materials in terms of climbing capability and power consumption, once the static friction and rolling resistance coefficients are estimated. The materials considered in this paper are ABS plastic of 74 Shore D hardness and Polyurethane of 50 Shore A hardness. This paper also intends to define which of these two materials is the most suitable for a climbing robot wheels according to the proposed parameters. The friction coefficients are measured by following a methodology derived from the standards ABNT NBR 16643:2017 and ABNT NBR 11992:2017 as well as from friction coefficient estimation works related to other application areas (Alió-Sanz *et al.*, 2016). The methodology is presented by Souza *et al.* (2021), not yet published.

It is worth noting that aluminium conductors are complex geometries formed by a number of smaller stranded wires. Therefore, analytical analyses or traditional friction measurement techniques, such as with tribometers, would lead to estimations that are not consistent with real operational conditions. Corrosion, wear, pollution, vibrations due to wind and locally scratched or broken strands may change the coefficient from any value measured in a completely controlled environment. Consequently, the methodology for friction measurement is applied using a wheel-prototype and other self-made apparatuses developed specifically to allow the experiments in real condition, a procedure that is commonly observed in other applications (Xu *et al.*, 2019; Chang *et al.*, 2016; Stawowiak and Żołnierz, 2018).

In order to accomplish the proposed goal, Section 2 presents how the maximum angle the robot can climb, the required torque and the power consumption are mathematically related to friction coefficients, proposing three criteria for material's proper comparison. Next, Section 3 describes the methodology used for friction coefficients estimation. The results obtained for robot wheels of ABS plastic 74 Shore D and Polyurethane 50 Shore A are discussed in Section 4 whereas Section 5 gives a summary of the main conclusions.

2. PARAMETERS DEPENDENT ON FRICTION

Based on vehicle dynamics and vehicle performance theories, some parameters dependent on rolling resistance and static friction coefficients are selected in order to objectively compare the materials. The choice of the wheel material must settle a compromise between power consumption and riding capability, i.e. the material must provide a friction coefficient high enough so that the robot is able to climb uphills and overcome obstacles, but not too high as to drastically decrease its autonomy. In this paper, the parameters used in the materials comparison are the maximum conductor angle in which the robot can stay parked; the required motor torque to traction the robot and the power dissipated due to the rolling resistance during robot ride.

The maximum inclination β in which an inspection robot can stay parked is given by the static friction coefficient μ between the wheels' surface and the surface of the wire cable. The reason behind this is that the braking force increases by the inclination angle. When the slope corresponds to an angle β, the braking force reaches its maximum magnitude and saturates (Jazar, 2017). Fig. 1 shows a schematic representation of the angle β, which is determined by:

$$\beta = \tan^{-1}(\mu) \tag{1}$$

It can be inferred from Eq. (1) that the higher the static friction coefficient μ, the greater the maximum angle β.

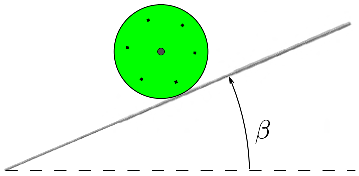

Figure 1. Schematic representation of the maximum inclination angle β that a riding cable robot stays parked

The motor torque T_f required to overcome the rolling resistance and the power P_f dissipated during the ride are indicated by the rolling resistance coefficient f (Jazar, 2017). T_f is given by:

$$T_f = fN_{wheel}r_d \tag{2}$$

where N_{wheel} is the normal force applied by the conductor to the robot wheel and r_d is the effective radius. Note that T_f is directly proportional to f, meaning that more torque is required to overcome the rolling resistance when the coefficient is higher.

The power loss during the ride is calculated through Eq. (3):

$$P_f = fN_{wheel}\frac{1}{i_t}\omega r_d \tag{3}$$

where ω is the motor angular speed and i_t is the transmission ratio. Similar to T_f, P_f linearly increases with the rolling resistance coefficient.

3. FIELD TEST METHOD TO MEASURE FRICTION

The method to measure the rolling resistance and the static friction coefficients between the surfaces of the robot's wheel and of the aluminum wire cable follows the inclined plane principle and was developed based on standards ABNT NBR 16643 and ABNT NBR 11992 and on the experiments conducted by Alió-Sanz *et al.* (2016).

3.1 Computation of the friction coefficient

A schematic representation of the field test arrangement is shown in Fig. 2(a). The field test is executed on a de-energized duplicate of a distribution power line, consisting of two poles with distinct heights connected by a real aluminum wire conductor used by the electricity utility for the state of Santa Catarina. A replica of the robot's wheel, made of the material whose friction properties is intended to analyze, is placed on the wire cable. The replica is held by a support installed behind it, preventing that the wheel rolls toward the shorter pole. A set of masses emulating the robot's weight is attached to the replica. A pulley is attached to the crossarm of the higher pole to be wrapped by an inextensible rope. One end of the rope is tied to the replica and the other one, to a container. The rope is submitted to traction until it becomes parallel to the conductor. Water is poured into the container until the wheel starts moving. In this manner, the maximum static friction force and the maximum rolling resistance can be determined from the water weight that started the replica's movement.

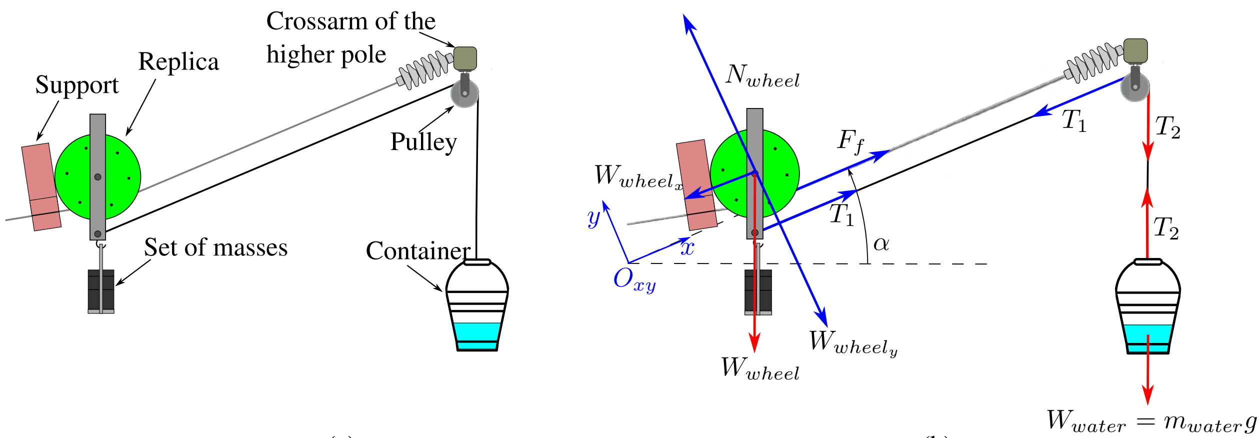

Figure 2. (a) Schematic representation of the field test arrangement and (b) forces involved in the experiment

The efforts maintaining the system in static equilibrium are shown in Fig. 2(b). The static friction and rolling resistance coefficients are computed from the replica's weight, W_{wheel}, the water weight W_{water} that broke the static equilibrium and the inclination angle α between the conductor/rope and the ground. There are four forces acting on the replica: its own weight W_{wheel}, a normal force N_{wheel}, a friction force F_f and a traction force T_1. According to the coordinate system O_{xy}, the replica's weight components at x and y directions, W_{wheel_x} and W_{wheel_y} respectively, are:

$$W_{wheel_x} = W_{wheel} \sin\alpha \tag{4}$$

$$W_{wheel_y} = W_{wheel} \cos\alpha \tag{5}$$

Since the replica is in static equilibrium, the y component of W_{weight} is equal to the normal force, i.e. $N_{wheel} = W_{wheel_y}$. Applying Newton's 2$^{\text{nd}}$ Law in x direction, the friction force F_f can be calculated as:

$$F_f = W_{wheel_x} - T_1 \tag{6}$$

The friction force is defined by the product $F_f = \varrho N_{wheel}$, where ϱ is a generic symbol that can represent the static friction coefficient, μ, or the rolling resistance coefficient, f. A generic symbol is adopted because both coefficients are calculated through the same equation. The meaning of ϱ is defined according to the motion state of the wheel replica. ϱ can be estimated by combining Eq. (4), (5) and (6):

$$\varrho = \frac{F_f}{N_{wheel}} = \frac{W_{wheel}\sin\alpha - T_1}{W_{wheel}\cos\alpha} \tag{7}$$

Note that the only unknown variable in the right side of Eq. (7) is T_1. W_{wheel} and α are measured during the test field, thus T_1 must be defined to compute ϱ. The second traction force T_2 helps to determine T_1. The water container is also in static equilibrium, so the traction force T_2 is equal to the container's weight:

$$T_2 = W_{water} = m_{water} g \tag{8}$$

where m_{water} is the mass of the container with water, measured right after the replica starts moving, and g the gravity acceleration.

The force T_1 is calculated via the quadratic equation shown in Eq. (9). The symbol f_b stands for the rolling resistance coefficient of the pulley's bearing, which is measured prior the field test. The deduction of Eq. (9) and the determination of f_b are detailed in Souza *et al.* (2021), not yet published.

$$(f_b^2 - 1)T_1^2 + 2T_2(f_b^2 \sin\alpha + 1)T_1 + (f_b^2 - 1)T_2^2 = 0 \tag{9}$$

Solving Eq. (9) results in two roots and the T_1 magnitude that gives the lowest friction force F_f in Eq. (6) should be used to estimate μ and f. The reason behind this choice is that the lower root represents the condition where the moment created by the friction between the pulley's shaft and the bearing (quantified by f_b) opposes the pulley's motion provoked by the container's weight. The higher root stands for the opposite effect, which has no physical meaning (Souza *et al.*, 2021).

3.2 Procedure of the field test

The field test is performed in an experimental apparatus based on the schematic view of Fig. 2(a) and shown in Fig. 3, built on a power network model used for tests at UFSC. The experimental apparatus is outdoors and it is recommended to execute the test fields on good weather. Since the tests are made outdoors, emulating the real surroundings of the robot operation, the resulting coefficients are valid for the average climate conditions of the city of Florianópolis, corresponding to an average room temperature of 21°C and an average relative humidity of 82%.

There are two frictional efforts opposing the robot's motion that can be assessed by the experiment: rolling resistance and static friction force. The rolling resistance is a force that arises when the wheel rolls over the conductor and it is evaluated by letting the wheel freely rotate around its own axis during the tests. The static friction force arises when the wheel slides on the conductor, so the wheel's rotation around its own axis is prevented in the tests in order to observe the static friction phenomenon.

The data collected from the field test are the angle α between the wire cable and the ground, established by the weight of the replica and the set of masses, and the container's mass m_{water} that breaks the equilibrium. The container weight is measured with a high-precision digital scale balance of the SF-400 model, whose scale has a measuring range from 1 g to 10 kg and a resolution of 1 g. The inclination between the rope and the ground is measured using the app *Pocket Bubble Level*, developed by ExaMobile S.A. for smartphones. Considering $g = 9.81 m/s^2$, the coefficients are estimated by replacing the data in Eq. (7) and (9). The rolling resistance coefficient of the pulley's bearing is determined before the field test and corresponds to $f_b = 0.1211$.

The friction coefficients are calculated for three different positions of the replica on the wire cable, to verify the effect of the cable sag generated by the replica's weight, as the sag decreases when the robot gets closer to the crossarm and α

Figure 3. Experimental apparatus in power network model at UFSC

increases. Besides, the conductor can have marked or broken strands that can influence the measurement in the region, so placing the replica on different positions allows to get an average result. The positions are defined in respect to the higher crossarm, as represented in Fig. 4. Ten repetitions are made for each position. The data measured during the field test are replaced in the equations detailed in Section 3.1 and both rolling resistance coefficient and static friction coefficient are computed for each repetition. The results are submitted to a statistics analysis, in which the average coefficient is calculated and scatter plots are generated.

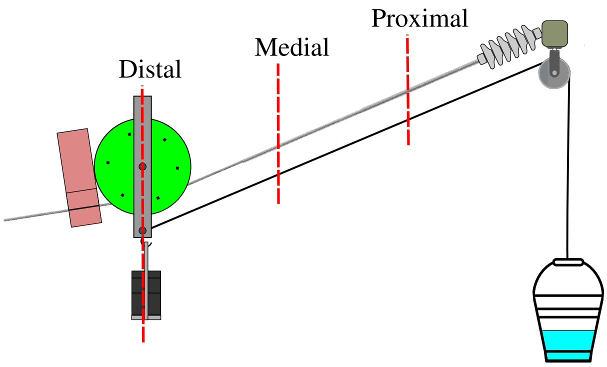

Figure 4. Three replica's position in relation to the higher crossarm

The set of masses standing for the robot weight weighs around 15 kg in the field tests quantifying the rolling resistance coefficient. The mass is reduced to 3.4 kg when the static friction coefficient is analyzed, since a higher mass would require more water to brake the static equilibrium, surpassing the balance scale.

4. FRICTION PROPERTIES OF POLYURETHANE AND ABS PLASTIC

There are two candidate materials to manufacture the inspection robot wheels: Polyurethane of 50 Shore A hardness (PU) and 3D printed ABS plastic of 74 Shore D hardness. The PU is milled into the shape of the wheel shown in Fig. 5(a) and a wheel is 3D printed in ABS plastic, presented in Fig. 5(b). Both wheels are submitted to the test field procedure described in Section 3.2. The test fields are carried out on dry and windless days. The test results are shown in the scatter charts of Fig. 6.

The chart of Fig. 6(a) presents the rolling resistance coefficient estimation for PU and ABS wheels. On average, the PU wheel has a rolling resistance coefficient of $f_{PU} = 0.074$, while the 3D printed wheel has a coefficient of $f_{ABS} = 0.049$. Note that f_{PU} is around 50% higher than f_{ABS}, what may be explained by the effect of the deformation on the rolling resistance: the higher the deformation, the greater the rolling resistance (Jazar, 2017). Since the ABS is harder than the PU, the ABS wheel undergoes less deformation than the PU wheel for the same load (the set of masses representing the robot weight), leading to a smaller f.

A smaller rolling resistance coefficient presents the advantages of requiring less motor torque to keep the robot motion

(a) (b)

Figure 5. Replicas of the robot wheel made of (a) Polyurethane of 50 Shore A hardness and (b) ABS plastic of 74 Shore D hardness

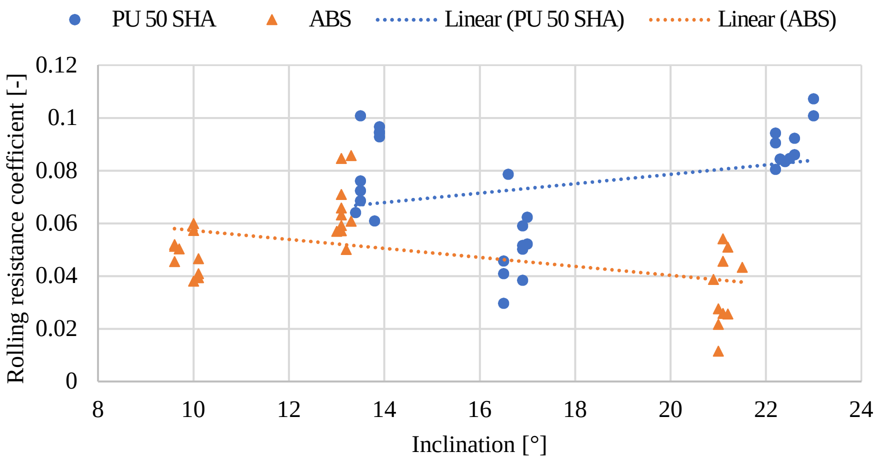

(a)

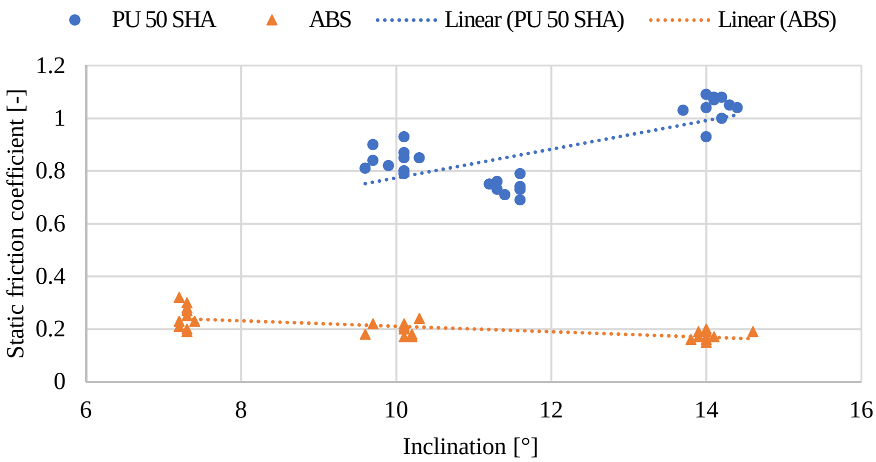

(b)

Figure 6. Scatter charts of the (a) rolling resistance coefficient and (b) static friction coefficient of the test field results for the PU and the ABS wheels. The average room temperature is 21°C and the average relative humidity is 82%.

and dissipating less power during robot ride. Considering an effective radius of $r_d = 52.5$ mm, a transmission ratio of $i_t = 5$, an angular speed of $\omega = 279$ rpm and an average normal force of $N_{wheel} = 148$ N on Eq. (2) and (3), the ABS wheel requires a torque of $T_{f_{ABS}} = 0.38$ Nm and causes a dissipation of $P_{f_{ABS}} = 2.25$ W. The PU wheel demands more torque besides dissipating more power, as replacing f_{PU} in Eq. (2) and (3) results in a torque $T_{f_{PU}} = 0.58$ Nm and a power loss of $P_{f_{PU}} = 3.39$ W, respectively. Supposing that the inspection robot has a traction motor with nominal load of 2.31 Nm whose magnitude is multiplied by $i_t = 5$, the ABS wheel requires a torque of around 3.3% of the nominal load to overcome the rolling resistance, while the PU wheel demands a torque corresponding to 5% of the nominal load. Assuming that the traction motor delivers a nominal power of 65.8 W, 3.4% of this power is dissipated due to the rolling friction between the ABS wheel and the wire-cable, while 5.1% would be dissipated if the wheel is made of PU.

Figure 6(b) contains the scatter chart estimating the static friction coefficient for PU and ABS wheels. The PU wheel presented an average static friction coefficient of $\mu_{PU} = 0.874$ while the ABS wheel presented a coefficient of $\mu_{ABS} = 0.205$. The chart of Fig. 6(b) graphically represents the contrast between the materials static friction coefficient. μ_{PU} is on average more than four times greater than μ_{ABS}, consequently the scatter plots of the PU and the ABS wheels do not superpose whatsoever and are distant from each other. The PU deformation capability is the reason behind the high static friction coefficient, as deformation is one of the mechanisms that generate friction (Jazar, 2017). The PU wheels deforms and fills the conductor irregularities during the test field, resulting in a higher friction force. Since the ABS is harder than the PU, the 3D printed wheel does not drape over the cable irregularities as much as the PU wheel does, leading to a lower friction force. As both wheels are submitted to the same load pressure (the set of masses weight), the static friction coefficients reflect the friction force difference.

Moreover, the disparity between the PU and ABS hardness, i.e. between μ_{PU} and μ_{ABS}, also impacts the maximum parking angle β. By replacing μ_{PU} on Eq. (1), it is estimated that the PU wheel can stay parked at a slope angle of $\beta_{PU} = 41.2°$. The ABS wheel cannot remain static at a such high inclination: applying μ_{ABS} in Eq. (1) results in $\beta_{ABS} = 11.6°$. Tab. 1 contains the parameters used to compare the performance of the PU and the ABS wheels.

Table 1. Friction properties of the PU and ABS wheels. The average room temperature is 21°C and the average relative humidity is 82%.

	PU	**ABS**
Rolling resistance coefficient f	0.074	0.049
Static friction coefficient μ	0.874	0.205
Average maximum parking angle β [°]	41.2	11.6
Average traction torque T_f [Nm]	0.58	0.38
Ratio between T_f and the nominal torque of 11.55 Nm [%]	5	3.32
Average dissipated power P_f [W]	3.39	2.25
Ratio between P_f and the nominal power of 65.8 W [%]	5.15	3.41

At first glance, the ABS could be considered more adequate than the PU to manufacture the wheel of a cable climbing robot. An ABS wheel dissipates less power during robot ride and reduces the torque demand, enabling to implement a lighter traction motor. However, the robot consumption cannot be single-handedly considered in the material selection. The inspection robot should be able to ride a wire-cable connecting uphill poles and to surpass obstacles such as insulators. The slope between poles in a real power distribution network can achieve an inclination close to 10° and the climbing angle can be greater during an obstacle overcoming. Thus an inspection robot with ABS wheels is submitted to a higher risk of slipping while trying to ride on the conductor or over-passing obstacles than a robot with PU wheels.

A compromise between climbing performance and power consumption must be reached when deciding if the inspection robot wheel will be made of PU or ABS. f_{PU} leads to higher power dissipation, but when compared to the motor nominal power, the difference between $P_{f_{PU}}$ and $P_{f_{ABS}}$ is less than 2 percentage points, which does not have a high effect on the robot's autonomy. Therefore, the wheel should be made of PU, which guarantees better climbing capability, even slightly increasing the consumption.

5. CONCLUSIONS

This paper assessed the comparison of materials intended for manufacturing wheels of cable riding robots, specially inspection robots for overhead distribution power lines. In this paper, two wheels made of materials with distinct hardness are compared: Polyurethane 50 Shore A hardness and ABS 74 Shore D hardness. The wheels are compared in terms of three different criteria: the maximum climbing inclination angle, the actuation torque required and the consequent power consumption.

By measuring the friction coefficients and calculating those criteria, it is observed that a compromise between climbing capability and motor capacity should exist. Analysing exclusively one criterion leads to misinterpretation and wrong design choices. This statement highlights the need for the deep and mathematical understanding of both the problem and how the design decisions impact the robotic system performance. Although the ABS wheel presented lower power consumption and would be the most suitable option for some applications, it can climb a maximum inclination of 11.6°. On the other hand, the Polyurethane wheel requires higher torque and power from the motor, but allows the robot to climb a slope angle higher than 40°. For the distribution line inspections, it occurs situations in which the angle of 11.6° is exceeded, leading to undesired slippage. Since the motor used meets the requirements for torque and power of both materials, the Polyurethane wheel is more suitable for this application as it provides a compromise between power consumption and climbing capability.

Future works include establishing additional comparison criteria for wheel materials, test fielding more materials and conducting tests with a robot prototype, to verify if the material performance does not degrade during the intended application. Other future work comprises performing the field test with the same materials analyzed in this paper, but in different weather conditions, in order to determine how each material behaves under climatic changes.

6. ACKNOWLEDGEMENTS

The R&D project that made this work possible was entitled "Development of a Robotized System for Inspection of Electricity Distribution Lines" (05697-0317 / 2017), regulated by ANEEL ("Agência Nacional de Energia Elétrica") and financed in Florianópolis - Brazil - by Celesc ("Centrais Elétricas de Santa Catarina"). This project is executed by the team of the Laboratory of Applied Robotics (LAR) from the Federal University of Santa Catarina (UFSC) and financially managed by FEESC ("Fundação de Ensino e Engenharia de Santa Catarina"). This study was financed in part by the Coordenação de Aperfeiçoamento de Pessoal de Nível Superior - Brasil (CAPES) - Finance Code 001 and by the Conselho Nacional de Desenvolvimento Científico e Tecnológico (CNPq) [grant number 142193/2018-6].

7. REFERENCES

ABNT NBR 11992, 2017. "Mangueiras de plástico para desobstrução e limpeza de tubulações de pvc rígido por hidrojateamento — determinação do coeficiente de atrito". Standard, Associação Brasileira de Normas Técnicas, Rio de Janeiro, RJ.

ABNT NBR 16643, 2017. "Microdutos - coeficiente de atrito - método de ensaio". Standard, Associação Brasileira de Normas Técnicas, Rio de Janeiro, RJ.

Alió-Sanz, J.J., Claros-Stucchi, M., Albaladejo, A., Iglesias-Conde, C. and Alvarado-Lorenzo, A., 2016. "In vitro comparative study on the friction of stainless steel wires with and without orthospeed®(jal 90458) on an inclined plane". *Journal of clinical and experimental dentistry*, Vol. 8, No. 2, p. e141.

Boje, E., 2014. "Modelling and control of a power supply for a power line inspection robot". In *Proceedings of the 2014 3rd International Conference on Applied Robotics for the Power Industry*. IEEE, pp. 1–6.

Bühringer, M., Berchtold, J., Büchel, M., Dold, C., Bütikofer, M., Feuerstein, M., Fischer, W., Bermes, C. and Siegwart, R., 2010. "Cable-crawler–robot for the inspection of high-voltage power lines that can passively roll over mast tops". *Industrial Robot: An International Journal*.

Chang, W., Yang, G., Yu, J., Liang, Z., Cheng, L. and Zhou, C., 2017. "Development of a power line inspection robot with hybrid operation modes". In *2017 IEEE/RSJ International Conference on Intelligent Robots and Systems (IROS)*. IEEE, pp. 973–978.

Chang, X.d., Peng, Y.x., Zhu, Z.c., Wang, D.g., Gong, X.s., Zou, S.y., Sun, S.s. and Xu, W.x., 2016. "Tribological properties of winding hoisting rope between two layers with different sliding parameters". *Advances in Mechanical Engineering*, Vol. 8, No. 12, p. 1687814016679911.

Debenest, P., Guarnieri, M., Takita, K., Fukushima, E.F., Hirose, S., Tamura, K., Kimura, A., Kubokawa, H., Iwama, N. and Shiga, F., 2008. "Expliner-robot for inspection of transmission lines". In *2008 IEEE International Conference on Robotics and Automation*. IEEE, pp. 3978–3984.

Goncalves, R.S. and Carvalho, J.C.M., 2015. "A mobile robot to be applied in high-voltage power lines". *Journal of the Brazilian Society of Mechanical Sciences and Engineering*, Vol. 37, No. 1, pp. 349–359.

Gulzar, M.A., Kumar, K., Javed, M.A. and Sharif, M., 2018. "High-voltage transmission line inspection robot". In *2018 International Conference on Engineering and Emerging Technologies (ICEET)*. IEEE, pp. 1–7.

Jazar, R.N., 2017. *Vehicle dynamics: theory and application*. Springer.

Jenssen, R., Roverso, D. *et al.*, 2018. "Automatic autonomous vision-based power line inspection: A review of current status and the potential role of deep learning". *International Journal of Electrical Power & Energy Systems*, Vol. 99, pp. 107–120.

Li, C., Wu, G. and Cao, H., 2009. "The research on mechanism, kinematics and experiment of 220kv double-circuit transmission line inspection robot". In *International Conference on Intelligent Robotics and Applications*. Springer, pp. 1146–1155.

Mirallès, F., Hamelin, P., Lambert, G., Lavoie, S., Pouliot, N., Montfrond, M. and Montambault, S., 2018. "Linedrone technology: Landing an unmanned aerial vehicle on a power line". In *2018 IEEE International Conference on Robotics and Automation (ICRA)*. IEEE, pp. 6545–6552.

Morozovsky, N. and Bewley, T., 2013. "Skysweeper: A low dof, dynamic high wire robot". In *2013 IEEE/RSJ International Conference on Intelligent Robots and Systems*. IEEE, pp. 2339–2344.

Mostashfi, A., Fakhari, A. and Badri, M.A., 2014. "A novel design of inspection robot for high-voltage power lines". *Industrial Robot: An International Journal*.

Nayyerloo, M., Yeganehparast, S.M.M., Barati, A. and Foumani, M.S., 2007. "Mechanical implementation and simulation of mobolab, a mobile robot for inspection of power transmission lines". *International Journal of Advanced Robotic Systems*, Vol. 4, No. 3, p. 41.

Pouliot, N. and Montambault, S., 2008. "Geometric design of the linescout, a teleoperated robot for power line inspection and maintenance". In *2008 IEEE International Conference on Robotics and Automation*. IEEE, pp. 3970–3977.

Prates, R.M., Cruz, R., Marotta, A.P., Ramos, R.P., Simas Filho, E.F. and Cardoso, J.S., 2019. "Insulator visual non-conformity detection in overhead power distribution lines using deep learning". *Computers & Electrical Engineering*, Vol. 78, pp. 343–355.

Qing, Z., Xiao-long, Z., Xin-ping, L., Jie, X., Ting, Z. and Cheng-jiang, W., 2016. "Mechanical design and research of a novel power lines inspection robot". In *2016 International Conference on Integrated Circuits and Microsystems (ICICM)*. IEEE, pp. 363–366.

Shakhatreh, H., Sawalmeh, A.H., Al-Fuqaha, A., Dou, Z., Almaita, E., Khalil, I., Othman, N.S., Khreishah, A. and Guizani, M., 2019. "Unmanned aerial vehicles (uavs): A survey on civil applications and key research challenges". *Ieee Access*, Vol. 7, pp. 48572–48634.

Souza, M.B., Fernandes, G.Q., Souza Vieira, R., Nicolazzi, L.C., Kinceler, R. and Dadam, A.P., 2021. "A methodology to field testing friction between aluminum wires and wheels of cable riding robots". In *26th ABCM International Congress of Mechanical Engineering*. ABCM. Unpublished.

Stawowiak, M. and Żołnierz, M., 2018. "Mobile test stand validation for measuring friction coefficient of carrying rope with friction lining". *Management Systems in Production Engineering*.

Wang, H., Li, E., Yang, G. and Guo, R., 2019. "Design of an inspection robot system with hybrid operation modes for power transmission lines". In *2019 IEEE International Conference on Mechatronics and Automation (ICMA)*. IEEE, pp. 2571–2576.

Xu, C.m., Peng, Y.x., Zhu, Z.c., Lu, H., Chen, G.a., Wang, D.g., Peng, X. and Wang, S.j., 2019. "Fretting friction and wear of steel wires in tension-torsion and helical contact form". *Wear*, Vol. 432, p. 202946.

Yang, D., Feng, Z. and Zhang, X., 2012. "A novel tribrachiation robot for power line inspection and its inverse kinematics analysis". In *2012 IEEE/ASME International Conference on Advanced Intelligent Mechatronics (AIM)*. IEEE, pp. 502–507.

Yifeng, S., Hongguang, W. and Lie, L., 2011. "Research on the influence of the driving wheel and robot posture on climbing capability of a transmission line inspection robot". In *2011 6th IEEE Conference on Industrial Electronics and Applications*. IEEE, pp. 1632–1639.

Zhang, B., Hou, J., Huang, G., Liu, X., Xue, D. and Wen, X., 2020. "Discussion on a new design of overhead transmission line inspection robot". In *2020 3rd International Conference on Robotics, Control and Automation Engineering (RCAE)*. IEEE, pp. 1–5.

8. RESPONSIBILITY NOTICE

The authors are solely responsible for the printed material included in this paper.